Probing the dynamic landscape of peptides in membrane mimics by synergized NMR experiments and MD simulations

Ricky Nencini,[†] Morgan L. G. Regnier,[†] Sofia M. Backlund,[†] Efstathia Mantzari,[†] Cory D. Dunn,[†] and O. H. Samuli Ollila[*,‡,†]

[†]*Institute of Biotechnology, University of Helsinki, Helsinki, Finland*

[‡]*VTT Technical Research Centre of Finland, Espoo, Finland*

E-mail: samuli.ollila@helsinki.fi

Abstract

Dynamic interactions between peptides and lipid membranes are crucial in many biological processes and biomedical applications However, monitoring of peptide dynamics in a membrane environment has been limited by the lack of experimental methods that could directly detect the fast (picosecond to nanosecond) timescale dynamics of peptides in this environment. Spin relaxation times from nuclear magnetic resonance (NMR) experiments are sensitive to such motions, but their applications are often limited by complications in sample preparation and interpretation of the data. Here we show that the detailed dynamic landscape of peptide-membrane mimics can be determined by a synergistic combination of solution state NMR experiments and atomistic resolution molecular dynamics (MD) simulations. Solution state NMR experiments are straightforward to implement without an excessive amount of sample, while direct combination of spin relaxation data to MD simulations enables detailed interpretation of the dynamic landscapes of both peptide and membrane mimics. The interpretation of NMR data from transmembrane, peripheral, and tail anchored peptides indicate that peptides and detergent molecules do not rotate together as a rigid body. Instead, peptides appear to rotate when placed in a viscous medium composed of detergent micelle. On the other hand, spin relaxation times also provide indirect information on peptide conformational ensembles. This work gives new perspectives on peptide conformational ensembles and dynamics in membrane environments.

Introduction

Dynamic interactions of peptides with membranes and other lipid aggregates are crucial in many biological functions and biomedical applications. For example, fusion peptides play an important role in virus entry into host cells,[1] antimicrobial peptides can be used as therapeutical agents,[2,3] signal peptides regulate protein translocation in cells,[4] and apolipoprotein mimetic peptides stabilize nanodiscs with potential pharmaceutical and other applications.[5,6] However, peptides are small and their dynamic interactions with membranes are difficult to capture by most experimental methods that access atomistic resolution data of biomolecular systems, such as crystallography or electron microscopy. Nuclear magnetic resonance (NMR) experiments are sensitive to fast (ps to μs) timescale motions of small molecules, but their applications are often limited by complications in sample preparation and in interpretation of the data.

Solid state NMR experiments have been useful in the detailed characterization of peptide interactions with membranes, yet they are inherently insensitive and thereby require large amounts of sample.[7–10] This combined with the lack of generally applicable straightforward and robust sample preparation protocols complicates many practical applications of solid-state NMR experiments. On the other hand, preparation of samples with peptides interacting with detergent micelles or more realistic membrane mimics, such as bicelles or nanodiscs, for solution-state NMR experiments is often more feasible and requires less material.[11] Even so, the interpretation of peptide-membrane interactions from solution state NMR experiments is often tedious because (i) reference direction defining the membrane plane that enables direct determination of order parameters is not well defined in solution state samples, and (ii) methods to interpret conformational ensembles and dynamics of aggregates of lipid-like disordered molecules from solution state NMR data are not available.

Spin relaxation times, T_1, T_2 and heteronuclear NOE relaxation (hetNOE), measured with solution state NMR from isotopically labelled ^{15}N atoms in peptide backbone are often used to determine protein dynamics by exploiting their connection to rotational dynamics of

N-H bond vectors via Redfield equations.[12,13] Spin relaxation times from proteins are typically interpreted using Lipari-Szabo formalism or its extensions, where bond vector rotational motions are assumed to compose of overall motion and one or more independent modes of internal motions, and parameters describing these motions are then solved by fitting to the experimental data.[13,14] However, for peptides embedded in disordered lipid-like aggregates, it is not clear which kind of rotational modes should be used in these calculations, and if all molecules in aggregates rotate together as a rigid object or if peptides rotate independently from other molecules. In addition, the number of molecules in each aggregate and the potential formation of dimers or higher multimers of peptides may affect rotational dynamics. To resolve all these free parameters by fitting would require a large amount of experimental data. On the other hand, complex heterogeneous dynamics of disordered molecules can be resolved by interpreting spin relaxation data directly using molecular dynamics (MD) simulations.[15] However, this approach requires careful exploration of MD simulation models that reproduce experimental spin relaxation times with sufficient accuracy for the interpretation of experimental data.[15,16]

Here we present an approach to resolve the dynamic landscape of complexes formed by disordered biomolecules by interpreting spin relaxation data from solution state NMR experiments using MD simulations. This is demonstrated for six different types of peptides embedded in SDS micelles, a standard anionic membrane-mimicking environment.[11] For the references, we resolved the dynamic landscape of two widely characterized peptides in the micellar environment: a model transmembrane GWALP peptide[17] and an antimicrobial Magainin 2 peptide that is known to settle in a peripheral orientation parallel to membranes.[2] To further demonstrate the usefulness of our approach, we studied tail-anchored peptides shown to target the mitochondrial outer membrane in yeast [eElaB(TA), eYqjD(TA), yFis1(TA)] or human [hMff(TA)] cells. The mechanism by which these tail-anchored peptides are inserted into lipid is still poorly understood.[18–20] For these six peptides, we predicted experimental spin relaxation times directly, without any further fitting, from the MD simulation force field

based on physical interaction parameters between atoms. Our predictions allowed detailed interpretation of the dynamic landscapes of peptides and a better understanding of their behaviour in lipid-like environments. Most importantly, the approach presented here can be generally applied to characterise dynamic landscapes of complexes formed by disordered biomolecules, including not only more realistic membrane mimicking systems, such as bicelles or nanodiscs,[5,6,11] but also to other systems such as lipid droplets[21,22] or membrane-less organelles.[23]

Results and discussion

Backbone ^{15}N spin relaxation times of peptides in micelles from NMR experiments

To experimentally characterize the dynamics of the selected six peptides in SDS micelle systems, we measured T_1, T_2, and hetNOE spin relaxation times of ^{15}N atoms that were specifically labelled in peptide backbone in positions shown in Fig. 1 a. All the labelled residues were visible in HSQC spectra with the exception of labelled N-terminal residues of hMff(TA) and yFis1(TA). HSQC spectra with the assignments and resulting spin relaxation times are shown in Figs 1 b and c, respectively.

For T_1 spin relaxation time, we observe an increasing trend in the order of eElaB(TA) < eYqjD(TA) < Magainin 2 < hMff(TA) < yFis1(TA) < GWALP, while the trend in T_2 is exactly opposite. Mitochondria-directed tail anchor proteins, eElaB(TA) and eYqjD(TA) derived from E. coli proteins have lower T_1 values and higher T_2 values than hMff(TA) and yFis1(TA) from humans and yeast. For peripheral Magainin 2 peptide, T_1 and T_2 times lay between values for tail anchors, while transmembrane GWALP has higher T_1 and lower T_2 values than any other peptide. HetNOE values lie between 0.4-1.0 for all the studied peptides, and systematic differences between peptides are not observed.

Spin relaxation times of ^{15}N are mostly sensitive to dynamics of N-H bonds in ps to

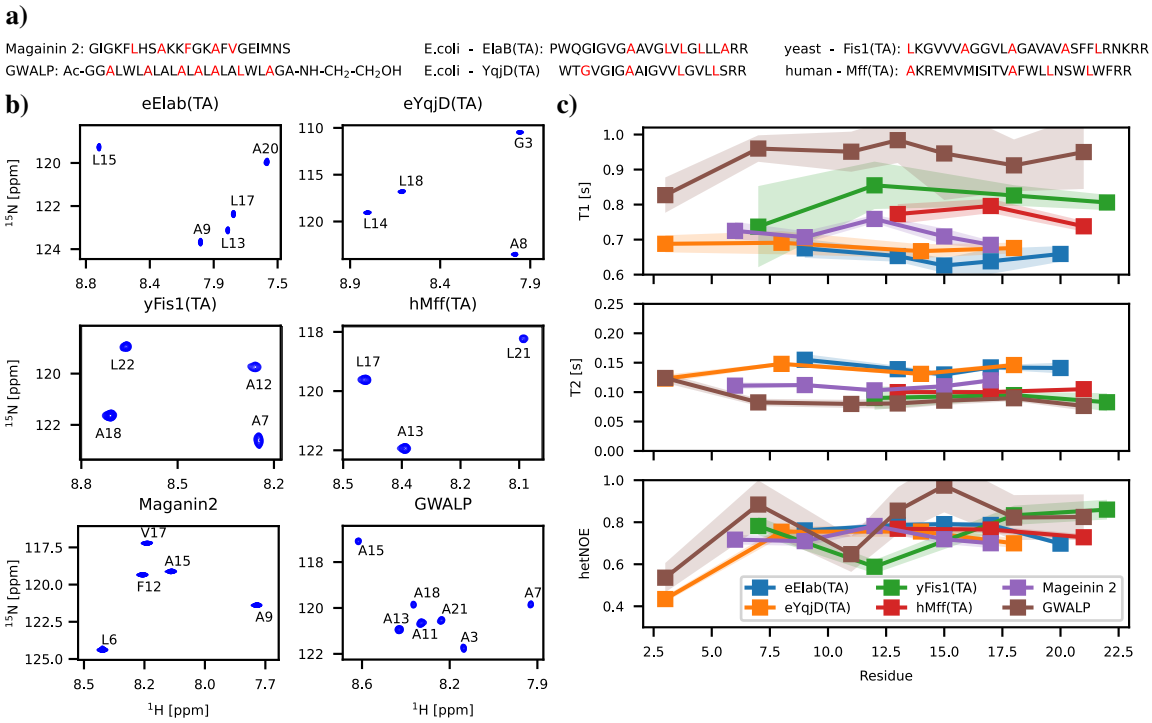

Figure 1: Experimental results for peptides in SDS micelles. a) Amino acid sequences with ^{15}N labelled residues shown in red for transmembrane GWALP23, peripheral Magainin 2, and mitochondria-directed tail anchor (eElaB(TA), eYqjD(TA), yFis1(TA), and hMff(TA)) peptides. b) ^{1}H - ^{15}N HSQC spectra and c) T_1, T_2 and hetNOE spin relaxation times measured from the peptides in SDS micelle and sodium-phosphate buffer at 310 K with 850 MHz spectrometer.

ns range in magnetic field dependent manner.[12] However, the interpretation of molecular dynamics from spin relaxation times is not straightforward, particularly for peptides in micelles where the detergent environment affects peptide dynamics in a non-trivial manner and standard models for protein dynamics may not be valid. Therefore, we rely here on interpretation from MD simulation models with detergents explicitly included in the following sections.

Predicting spin relaxation times of micelles from physical interactions between atoms using MD simulations.

To interpret the molecular dynamics from the measured NMR spin relaxation times, we set out to perform MD simulations that reproduce the experimental spin relaxation times without any further fitting, and thereby directly provide interpretation for the experimental data. Because Amber-based force fields with water models derived from TIP4P were previously successful in such tasks for partially disordered proteins,[15] we first simulated an SDS micelle in water with parameters from AmberTools.[24] However, this micelle proceeded to a gel-like phase with slow dynamics and deuterium spin relaxation times diverging from experimental data obtained from the literature[25] (Fig. 2). On the other hand, another popular protein force field with SDS parameters available, CHARMM36,[26] is parameterized with the TIP3P[27] based water model, which suffers from low water viscosity and overly rapid dynamics, leading to incorrect spin relaxation time values that do not relate well to data obtained by experiments.[16] This is indeed observed also in our simulations in Fig. 2. Therefore, we proceeded to use CHARMM36 parameters with OPC water model[28] that has a viscosity value in good agreement with experiments.[29] This combination has been previously shown to give reasonable results for bilayers and monolayers.[30,31] Indeed, SDS micelles simulated with CHARMM36 parameters and the OPC water model remain in a fluid-like phase and predict deuterium spin relaxation times that are in good agreement with experiments (Fig. 2). Therefore, we proceeded to simulations with peptides in micellar environments using the CHARMM36 parameters with the OPC water model.

Predicting spin relaxation times of peptide-micelle complexes from physical interactions between atoms using MD simulations.

Besides the force field parameters, the number of SDS molecules per micelle has to be set manually in molecular dynamics simulations, because simulations of spontaneous aggregation

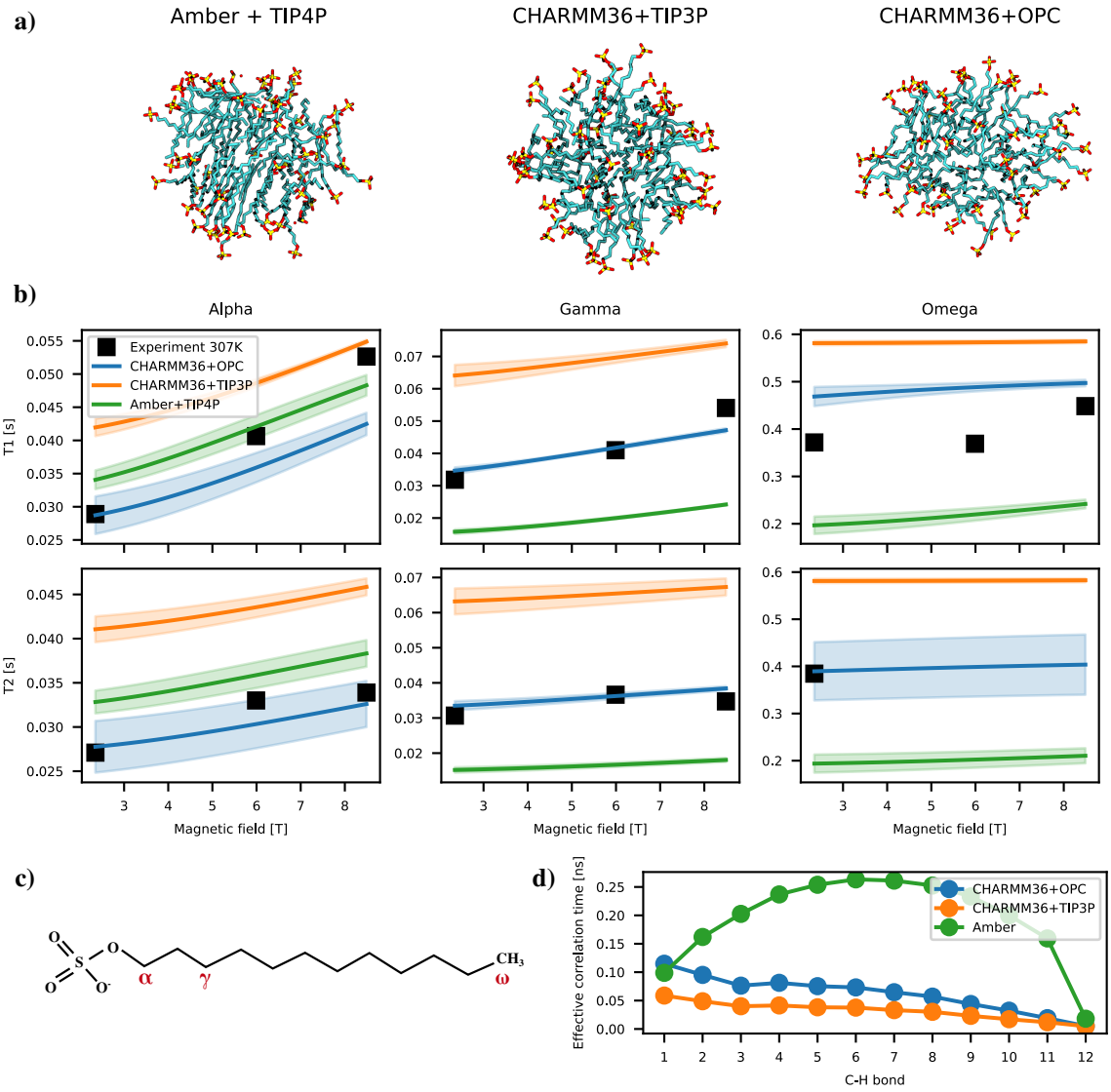

Figure 2: Spin relaxation times of SDS micelles in water at 307 K. a) Snapshots from MD simulations showing the gel-like phase for Amber simulations and liquid-like phase for CHARMM36 simulations. b) Deuterium T_1 and T_2 spin relaxation data from experiments[25] and MD simulations for isotopically labelled α, γ and ω segments. c) Chemical structure of SDS with the assignment of labelled segments. d) Effective correlation times, τ_{eff}, of each C-H bond in SDS molecules from MD simulations.

in large systems are not feasible at atomistic resolution. For preliminary screening, we simulated each peptide in a micelle with the sizes of 40, 45 and 50 SDS molecules for about 300 ns. In this quick scan, systems with 50 SDS molecules reproduced the experimental spin relaxation data quite well for all the peptides except GWALP. Due to the substantial computational cost, we performed a more systematic study on the micelle size dependence only for hMff(TA) which indicated the strongest size dependence in the initial screening. For this, we simulated hMff(TA) in micelles with 40, 45, 50, and 60 SDS molecules. Each system was simulated for at least 3 μs and repeated 3 times from different initial configurations. The results in Fig 3 a) show systematic but weak dependence of T_1 on micelle sizes, while T_2 and hetNOE spin relaxation times from differently sized micelles are mostly within the error bars. Based on these results, we ran three independent simulations of each peptide except GWALP with 50 SDS molecules for at least 3 μs each. Spin relaxation times from these simulations were close to experimental values with the exception of eElaB(TA) for which T_1 was slightly overestimated and T_2 slightly underestimated (Fig. 3). Therefore, eElaB(TA) simulations were repeated also in micelles with 40 SDS molecules, which indeed gave T_1 and T_2 values significantly closer to experiments, see Figure 3 d).

To understand the origin of large T_1 and small T_2 values in GWALP experiments, we screened the dependence on micelle size up to 80 SDS molecules per micelle for this peptide. Furthermore, we investigated whether dimerization could explain distinct spin relaxation times for GWALP by simulating two peptides in micelles with different numbers of SDS molecules. Results in Fig. 3 show that we can reproduce the experimental T_1 spin relaxation data either with one GWALP peptide in a micelle with 80 SDS molecules or with two GWALP peptides in a micelle with 70 SDS molecules. For systems with two GWALP peptides in an SDS micelle, we observe two different scenarios: peptides either strongly interact with each other, creating a dimer that rotates in the micelle as one entity, or the two peptides continue to rotate independently, see Figs. S1 a) and b) in the supplementary information. We observe slight differences between these two scenarios in terms of T_1 spin relaxation times.

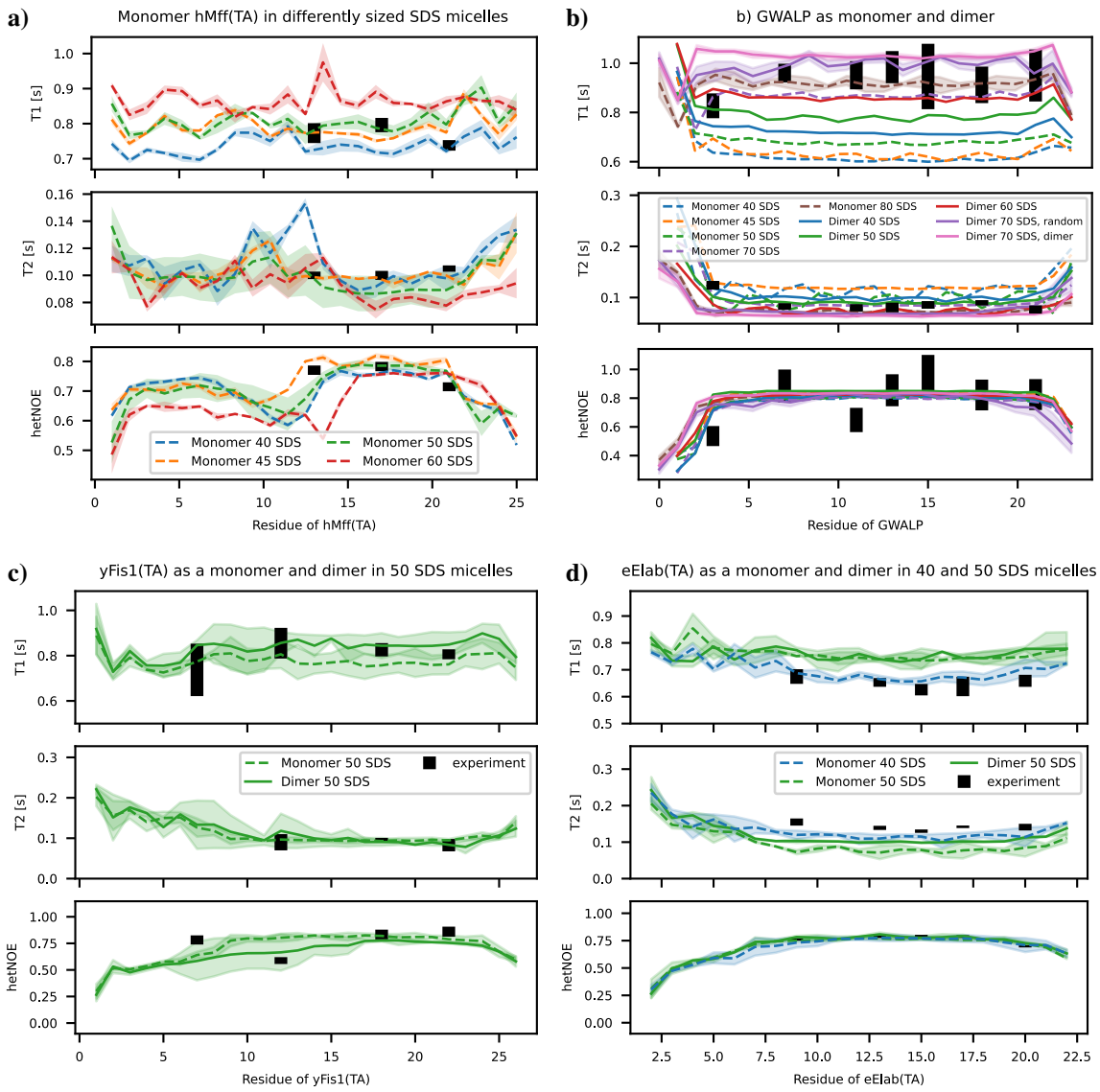

Figure 3: Effect of micelle size and dimerization on spin relaxation times. a) Spin relaxation times of hMff(TA) peptide as a function of SDS micelle size. The dashed line shows the average over 3 replicas simulated with 1 peptide per micelle. The shaded region is the standard error of the mean calculated from the 3 simulations. b) Spin relaxation times of GWALP peptide as a monomer or dimer as a function of the SDS micelle size. c) Spin relaxation times of yFis1(TA) peptide in a micelle with 50 SDS molecules as a monomer or dimer. For the dimer, a solid line shows the average over the 2 peptides in a micelle in one simulation. For the monomer, the dashed line is the average taken over 3 replicas. Shaded regions are the standard errors of the mean. d) Spin relaxation times of eElaB(TA) peptide in a micelle with 50 SDS molecules as a monomer or dimer, and in a micelle with 40 SDS molecules as a monomer.

While two independently rotating GWALP peptides in a micelle with 70 SDS molecules reproduce the experimental results slightly better, peptides rotating in a correlated manner would probably reproduce the experimental data equally well after a slight decrease in the number of SDS molecules. To also check the effect of dimerization on spin relaxation times in other peptides, we run simulations with two eElaB(TA) or yFis1(TA) molecules in one micelle. Differences between systems having one or two peptides in a micelle were smaller for eElaB(TA) and yFis1(TA) than for GWALP (Figs. 3 b)-d)), and interactions between two peptides were observed neither for yFis1(TA) nor eElaB(TA), see Figure S1. In conclusion, our results suggest that distinct spin relaxation times for GWALP systems in experiments can be explained by their presence in larger aggregates, yet we cannot distinguish with the current data whether there are one or two peptides in each micelle. However, GWALP dimers seem slightly more probable than for other peptides as they sometimes dimerize spontaneously and dimers remain stable in simulations.

Spin relaxation times and representative snapshots from the systems that predict values closest to experiments are shown in Figs. 4 a) and b), respectively. These simulations reproduce the main experimentally observed differences in spin relaxation times between the peptides, particularly the increase of T_1 values in the order of eElaB(TA) $\lesssim$ eYqjD(TA) $\lesssim$ Magainin 2 $<$ hMff(TA) $\lesssim$ yFis1(TA) $<$ GWALP. Notably, after selecting the force field parameters and the number of molecules in the simulation system, no further fitting is made to reproduce the experimental data. Therefore, the selected simulations predict experimental spin relaxation times directly from physical interactions between atoms with relatively good accuracy, which justifies their further usage in interpreting the dynamic landscape of peptides in micellar environments performed in the next sections.

Dynamic landscape of peptide-micelle complexes

To provide detailed interpretations of dynamic landscapes of peptide-micelle complexes, we describe the relevance of different timescales for the protein rotation by determining how

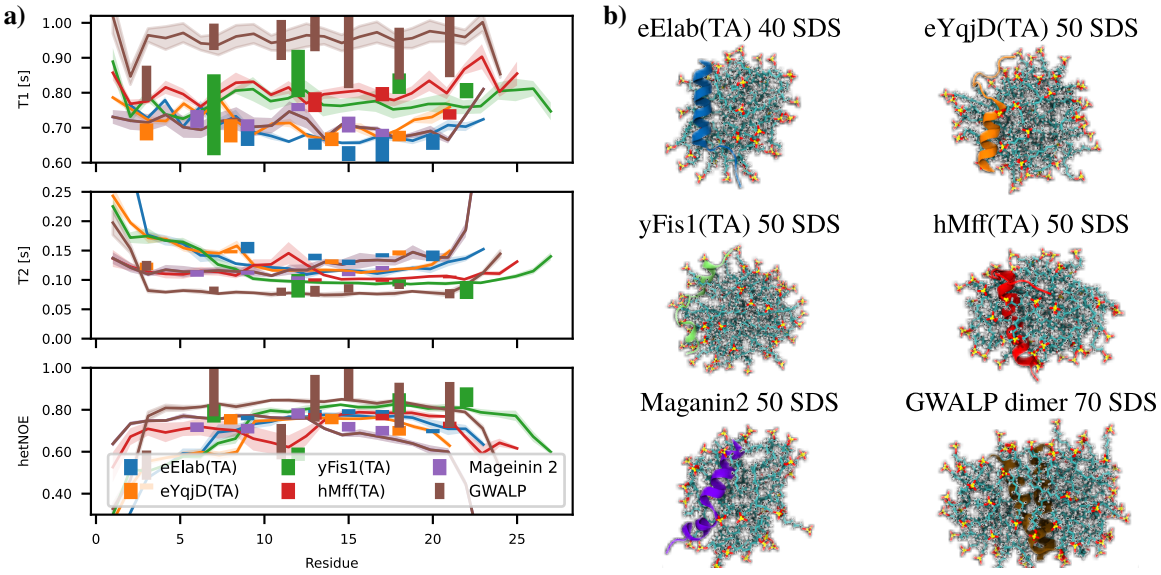

Figure 4: Spin relaxation times from the best simulations compared with experiments. a) Spin relaxation times from the best simulations and experiments. Experimental values are in the middle of the shown rectangles and the edges represent the experimental error. The lines represent an average over 3 simulation replicas and the shaded region shows the error of the mean. b) Representative snapshots of the studied peptides in SDS micelles.

much each timescale contributes to the rotational relaxation of each bond. To this end, we exploit the weights of different timescales resulting from the fit of exponential functions (Eq. 2) to the rotational correlation functions of N-H or C-H bonds (Eq. 1) calculated from simulations that give the best predictions for experimental spin relaxation times in Fig. 4. Because the resulting combination of weights and timescales reproduce experimental spin relaxation times, they can be considered as an interpretation of the dynamic landscape detected by the experiments. Notably, this direct approach (i) is free from the assumptions about the number of relaxation processes or their timescales, (ii) does not require the re-scaling of inaccurate simulation data that is required when using common methods to interpret dynamics from spin relaxation data,[13,14,32–34] and (iii) provides a higher resolution and intuitively more comprehensible interpretation than the dynamical detector analysis.[35] We have previously reported similar analyses for pure protein[15,16] and lipid[36] systems.

The full dynamic landscapes for proteins with all observed timescales and their weights are shown in Fig. S2 in the supplementary information, while a more comprehensible pre-

sentation where the weight of each timescale is represented by the point size is shown in Fig. 5 for peptides and SDS molecules. For all the peptides, we observe dominant rotational timescales between approximately 5 and 9 ns, with weights above approximately 0.5 for most residues. These dominant timescales can be interpreted to correspond to the overall rotational dynamics of peptides. The fastest dominant timescales around 5 ns are observed for eElaB(TA) and eYqjD(TA), and Magainin 2, although the C-terminal half of Magainin 2 has even faster timescales around 4 ns. Dominant timescales of hMff(TA) and yFis1(TA) are slightly slower with values just above 6 ns, while GWALP exhibits significantly slower rotational dynamics than other peptides with dominant timescales of approximately 8 ns. Because the differences in dominant timescales between peptides correlate with the differences in T_1 times, we conclude that the experimentally observed differences in T_1 values arise from differences in overall rotational dynamics between peptides.

Similar analysis of dynamic landscapes of SDS molecules in Fig. 5 b reveals substantially different behaviour than for peptides: Dynamics is dominated by timescales below 100 ps, and nanosecond timescale motions related to overall rotation of peptides are not observed for detergents. This suggests that the motions of peptides and SDS are not concerted, but peptides rotate independently from detergent molecules in a viscous media formed by the micelle. We further investigated the coupling between micelle and peptide dynamics by comparing the peptide dynamics observed in MD simulations to the prediction from the Stokes-Einstein equation, assuming that the peptide-micelle complex rotates as a rigid body with a fixed radius in an environment having the viscosity of water. The Stokes-Einstein equation predicts significantly faster peptide dynamics and stronger dependence on the micelle radius than is observed in simulations, as shown in Fig 6. For example, in the case of the hMff system in 50 SDS molecules, the gyromagnetic radius calculated from the simulations is 1.6 nm. However, to obtain the rotational timescales observed in simulations from the Stokes-Einstein equation, the radius of the micelle would have to be 3.0 nm, which is almost twice as large as the value from the simulations. On the other hand, the viscosity value

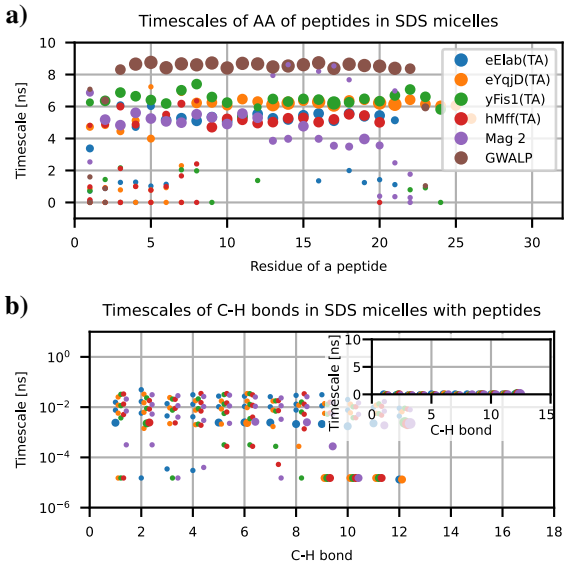

Figure 5: Dynamic landscape of a) peptides and b) SDS molecules from the simulations in the best agreement with experiments in Fig. 4. The point sizes represent the weight of each timescale in the rotational relaxation process.

in Stokes-Einstein equation should be 7.5 mPa s to obtain the same dynamics as observed in simulations, which is approximately ten times larger than the viscosity of water at 310 K (approximately 0.69 mPa s).

In conclusion, our results indicate a dynamic conception of peptide-micelle complexes where the rotation of peptides is dominated by nanosecond timescale dynamics related to their overall motion that can be experimentally detected by T_1 values. Because peptides rotate independently from detergents in a viscous media formed by the micelle, the rotation of the peptide-micelle complex cannot be described by the Stokes-Einstein equation that assumes that peptides and detergents rotate together as a spherical rigid body.

Correlations between spin relaxation times and biophysical properties of peptide-micelle complex

Spin relaxation times measured here are sensitive to the rotational dynamics of peptide backbone N-H bonds, yet these dynamics depend indirectly also on conformations sampled by the peptides. Therefore, spin relaxation times are potential proxies also for conformational

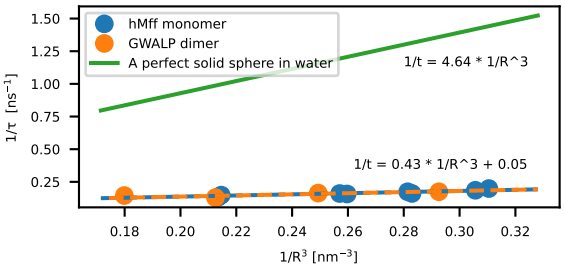

Figure 6: Rotational dynamics of peptides as a function of micelle size (radius of gyration) from Stokes-Einstein equation (green line), and from MD simulations of hMff(TA) as a monomer and GWALP as a dimer in micelles with different numbers of SDS molecules.

ensembles of peptides which is the case for example for partially disordered proteins.[15] To investigate if spin relaxation times could be useful to characterize peptide conformations also in the micellar environment, we analyzed correlations between peptide helicity and spin relaxation times in Fig. 7.

In simulations of individual systems, such as yFis1(TA) peptide in a micelle with 50 SDS molecules shown in Figure 7 a), helical regions have high hetNOE values and lower T_2 values than non-helical regions, while the changes in T_1 values are less clear. To investigate the generality of such correlations, we plotted the spin relaxation times as a function of the peptide helicity from all simulations listed in Tables S2 and S3 into Figure 7 b). This analysis reveals that helicity correlates with T_2 and hetNOE values with Pearson correlation coefficients of -0.57 and 0.79, respectively, while the correlation with T_1 values is weaker with a Pearson correlation coefficient of -0.15. However, spin relaxation times depend also upon other properties besides helicity that vary between systems, such as micelle size. Therefore, we also calculated Pearson correlation coefficients between helicity and spin relaxation times separately for each individual simulation in Fig. 7 c). In all individual simulations, correlation coefficients between helicity and hetNOE values are above 0.5, with p-values below 0.05. In the case of T_2 values, all the systems have correlation coefficients with helicity below -0.45 with p-values below 0.05 except for three systems (two replicas of hMff(TA) with 45 SDS molecules and a GWALP monomer with 50 SDS molecules) for which significant correlation was not found (correlation coefficients around -0.25 with p-values around 0.2). In the case

of T_1 values, negative correlation with helicity with correlation coefficients below -0.5 and p-values below 0.05 are common, yet significant correlation is not found in many systems and some systems have also significant positive correlation.

In conclusion, our results suggest that the residues with large hetNOE and small T_2 values have a higher tendency to form helices with respect to other residues within the same peptide. Similar correlations are observed also across different peptides, yet they are weaker because also other factors, such as micelle size, play a role. On the other hand, correlations of T_1 values with the helical tendency is less straightforward.

Conclusions

We show that MD simulations based on physical models can predict experimental ^{15}N spin peptide backbone relaxation times in detergent systems without any further fitting. Our MD simulations with the correct number of molecules and realistic force field parameters capture experimental spin relaxation times for peptides with different sequences within experimental error bars for almost all labelled residues in the tested systems. Therefore, our results suggest that MD simulations can be used as a highly powerful tool to interpret experimental spin relaxation time data from lipid-protein aggregates with high spatiotemporal resolution. Our direct combination of MD simulation models and NMR data avoids indirect comparisons between two different models, i.e., a model used to interpret spin relaxation data vs. MD simulation model, that is done in many currently used methods.[38] On the other hand, our approach is free from assumptions about the number and timescales of rotation modes present in the system, as well as from arbitrary scaling of simulation results that are required to interpret spin relaxation time data and reproduce experimental results when deploying other methods.[14,32–34,38] These advances enable the interpretation of spin relaxation times for systems that are beyond the scope of current approaches due to the large amounts of data required for parameter fitting, such as complex protein aggregates containing lipids or

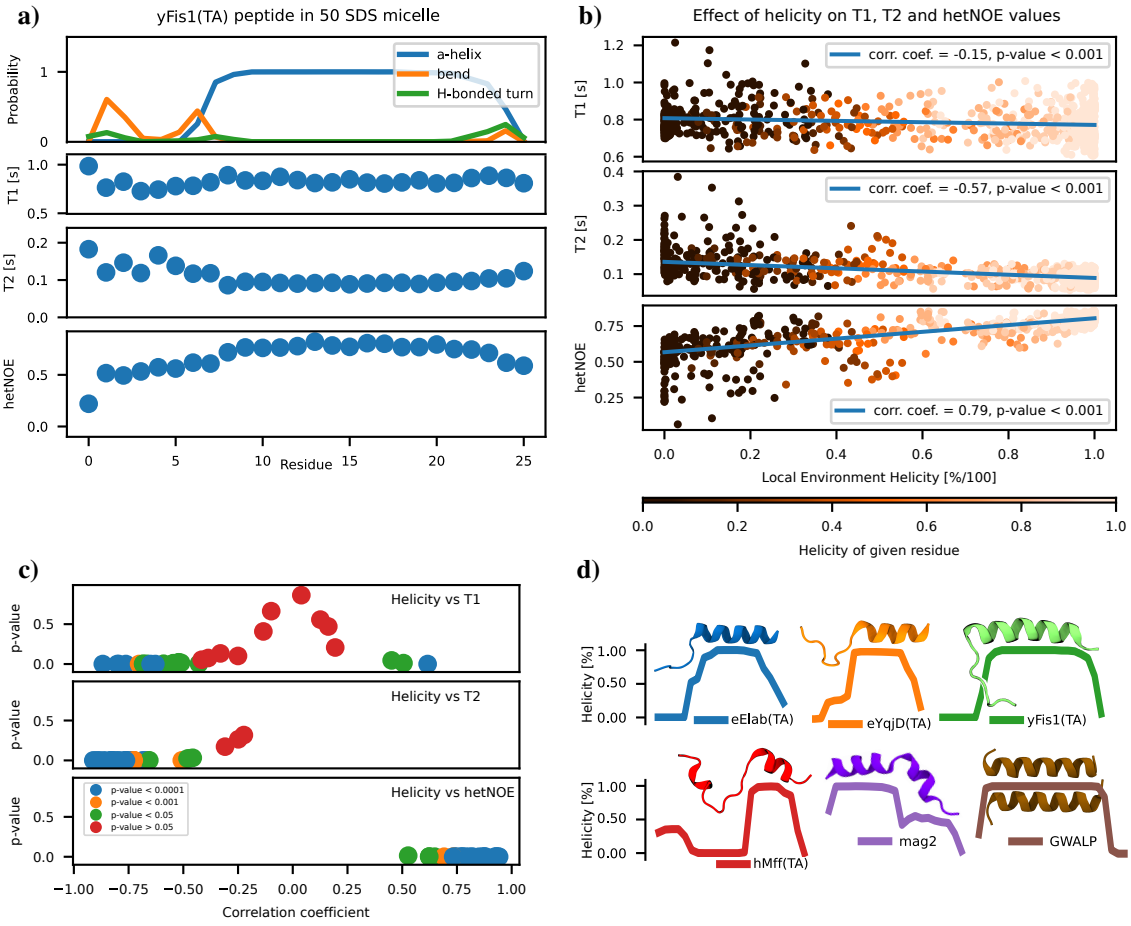

Figure 7: Correlations between helicity and spin relaxation times of peptides. a) Three most abundant secondary structures detected by DSSP[37] analysis and spin relaxation times from a simulation of yFis1(TA) in a micelle with 50 SDS molecules. b) Scatter plot and Pearson correlation coefficients between helicity and spin relaxation times from individual residues in all simulations listed in tables S2 and S3. The local environment helicity on the x-axis is the average over the given residue and the left and the right neighbouring residue if these exist. The colour of a point then encodes for the helicity of the given residue without neighbour averaging. c) Pearson correlation coefficients and their p-values between the residual local environment helicity and spin relaxation times calculated separately for individual simulations. d) Average helicities over three replicas with representative snapshots from MD simulations.

detergents.

To demonstrate the practical advances of our approach, we determined the dynamic landscape of peptide-detergent aggregates for the first time. Our findings support a view of peptide dynamics within a detergent matrix in which peptides and detergent molecules do not rotate together as a rigid body in solvent. Rather, peptides rotate in a viscous medium composed of detergent micelle. Based on our interpretation of peptide backbone ^{15}N spin relaxation times, the rotation of analyzed peptides in detergent aggregates was dominated by timescales between approximately 4-8 ns which we interpret to arise from the overall rotation of peptides. We explain the substantially slower overall rotation observed for transmembrane GWALP peptide, with the timescale of ∼8 ns, by its preference for larger detergent aggregates than peripheral Magainin 2 or mitochondria tail anchor peptides having overall rotational timescales of ∼4-6 ns. This result supports previous studies suggesting that mitochondria tail anchor peptides are more similar to peripheral peptides than transmembrane peptides.[19,39–41] On the other hand, the rotational dynamics of SDS molecules forming the detergents is dominated by timescales faster than 100 ps while ns timescales dominating in embedded peptides are absent.

Furthermore, we used our approach to understand indirect relations between peptide backbone ^{15}N spin relaxation times and conformational ensembles. We found significant correlations of helical propensities of peptide residues with large hetNOE and low T_2 values, particularly when compared with the other residues within the same peptide. On the other hand, T_1 values mainly correlated with the overall rotation of peptides. These relations enable rapid interpretations of peptide conformations in detergent aggregates from spin relaxation times even when MD simulation data is not available.

The advantages of our direct combination of NMR experiments and MD simulations are demonstrated here for peptides in SDS detergent micelles, yet the presented approach can be applied to any biomolecular aggregate for which experimental spin relaxation times are accessible and realistic MD simulations can be performed. This includes many systems

that are difficult to characterize by currently available experimental methods, such as fully or partially disordered proteins,[15] bicelles or nanodiscs,[5,6,11] membraneless organelles,[23] and lipid droplets.[21,22] In addition to the interpretation of experimental NMR data, the presented approach will be useful also for the evaluation and improvement of MD simulation quality. In the era of data science and machine learning, such benchmark data is becoming increasingly important and endeavours to define such data for proteins and lipids are ongoing.[42–44]

Materials and Methods

NMR experiments

Peptides with the selected alanine, phenylalanine, glycine, or leucine having ^{15}N labels in the backbone (positions shown in Fig. 1) were purchased from Peptide Protein Research Ltd (United Kingdom) in a powder form with the purity above 95%. Approximately 0.3 mg of each peptide was weighed in an eppendorf vial using an analytical balance (Precisa, XT 120A). The powder was then dissolved with deuterated sodium dodecyl sulfate (SDS, Sigma Aldrich) to obtain a solution with 0.3 mM peptide in 30 mM SDS and 20 mM sodium-phosphate buffer. 5% D_2O was added for the lock in the NMR spectrometer. The solvent was prepared dissolving approximately 4.2 mg of SDS with 337.5 μl of milli-Q water, 90 μl sodium-phosphate buffer (pH 7.4, 0.1 M) and 22.5 μl of D_2O. The samples were transferred into 5 mm NMR tubes and all the NMR measurements were performed at 310 K using on Bruker Avance IIIHD 850 MHz spectrometer equipped with a cryogenically cooled probe head at the Institute of Biotechnology, University of Helsinki.

To assign the peaks from labelled amino acids, we measured [^{1}H,^{15}N]-HSQC (2048 points in the F3 domain, 128 points in the F2 domain, 16 scans, and recycling delay of 1.1 s between scans), [^{1}H,^{1}H]-TOCSY (1536 points in F3 domain, 512 points in F2 domain, 16 scans, mixing time of 60 ms), and [^{1}H,^{1}H]-NOESY spectra (1536 points in F3 domain, 512 points in F2 domain, 16 scans, mixing time of 280 ms). A recycling delay of 2.1 s was used between scans

and the ^{1}H carrier frequency was positioned at 4.703 ppm for both TOSCY and NOESY measurements. The spectral widths were 14.0 ppm (^{1}H, F1) and 10.2 ppm (^{1}H, F2) for [^{1}H,^{1}H]-TOCSY and 10.2 ppm (^{1}H, F1) and 10.2 ppm (^{1}H, F2) [^{1}H,^{1}H]-NOESY. For HSQC spectra, the ^{1}H carrier frequency was positioned at 4.703 ppm, the ^{15}N carrier frequency at 119 ppm, and the spectral widths were 12.0 ppm (^{1}H, F2) and 33.0 ppm (^{15}N, F1). All these experiments were processed and analyzed using CcpNmr Analysis software (version 3.0.3).[45] For the assignment, the complete spin systems of the amino acid residues were first identified using their proton-proton J-couplings ([^{1}H,^{1}H]-TOCSY) combined with their proton-nitrogen J-coupling ([^{15}N,^{1}H]-HSQC). These spin systems were then located within the peptide sequence by means of through-space, sequential NOE connectivities between adjacent residues.[46]

Spin relaxation times were acquired with standard pulse sequences[12,47,48] using 1664 points in the F3 domain, 300 points in the F2 domain, and 8 scans. Delay times were set to 20, 50, 100, 200, 300, 500, 700, and 900 ms for T_1, and 34, 51, 68, 85, 119, 153, 187, 220, and 254 ms for T_2. The recycling delay of 3.5 s between scans was used for both T_1 and T_2, and 5 s for heteronuclear NOE. The spectral widths were the same as in HSQC experiments. The T_1 and T_2 relaxation data were processed and analyzed using Bruker Dynamic Center software (version 2.7.2). For the analysis of hetNOE spin relaxation times, peak heights were determined by TopSpin software from spectra with and without NOE. To determine the errors for hetNOEs, signal to noise ratio was first determined from the region without any peaks, and the limiting extremes of the noise values were then added to or subtracted from the peaks to estimate the largest effect of noise to the ratio between the peaks in the two spectra.

MD simulations

Simulated systems

SDS micelles in water without peptides were simulated using Amber parameters from AmberTools[24] and CHARMM36[26] parameters from CHARMM-GUI.[49,50] Following the electronic continuum correction (ECC) to implicitly include electronic polarization, atom charges were scaled by factor 0.75 in Amber simulations[51] and compatible ion parameters were used.[52] Amber simulations were ran with TIP4P[27] and CHARMM36 simulations with TIP3P[27] (CHARMM version), OPC,[28] or TIP4P[27] water models. We first simulated SDS micelles at 298 K and 307 K with the standard saving frequency of 10 ps for coordinates for 362-1809 ns. Because SDS molecules had a substantial amount of rotational dynamics with faster timescales than the saving frequency, we initiated simulations with the saving frequency of 0.01 ps using conformations at different timepoints from the first simulations as the starting configurations. Simulated systems of SDS micelles without peptides and their starting configurations are listed in Table S1.

To construct the initial configurations of peptides in micelles, peptide PDB files were first generated using ProBuilder server `https://www.ddl.unimi.it/vegaol/probuilder.htm`, and then embedded to SDS micelles using CHARMM GUI.[49,50] Systems were hydrated with approximately 24 000-40 000 water molecules and the total charge was neutralized with sodium ions. To test the potential dependence of the results on simulation box size, we ran hMff(TA) simulations with different box sizes, see Fig. S4 in the supplementary information. We observed mild dependence on simulation box size with systems less than approximately 39 000 water molecules. This should be taken into account when planning the simulations, or concluding optimal micelle sizes from simulations with less amount of water than this. Simulation replicas were initiated from different time points of the first simulation for each system with a new random set of starting velocities. Further details are given in Table S2.

Starting configurations for simulations with two GWALP, yFis1(TA), or eElaB(TA) pep-

tides within the same micelle were prepared by (i) removing water molecules from an equilibrated snapshot of a monomeric system, (ii) adding a second peptide to close proximity of the micelle, (iii) solvating the system again. For the GWALP peptide, such simulations were run with 40, 45, 50, and 60 SDS molecules. In the simulation with 50 SDS molecules, two GWALP peptides started to interact with each other and created a dimer where the two peptides rotated together in the micelle, see Figure S1 d). Therefore, with the optimal micelle size of 70 SDS, we ran replicas starting from conformations with (together) and without (separate) mutual interactions of two GWALP peptides. In all of the "together" simulations, peptides stayed in the form of the dimer for the whole length of the simulations. One of the systems with a "separate" starting configuration indicated potential dimer formation at the end of the simulation, while peptides retained independent motions otherwise. Simulations with systems having two peptides in the same micelle are summarized in Table S3.

The convergence of systems was monitored by calculating the number of SDS molecules in each micelle as described below, for example of equilibrated system see Fig. S3. We also ensured by visual inspection that all peptides were incorporated into micelles. Only the converged parts of trajectories were used for the analyses.

Simulation details

All simulations were performed using Gromacs versions 2021.1, 2021.5, and 2022.2.[53,54] Parameters from AmberTools were converted to Gromacs format using ACEPYPE.[55] Standard CHARMM-GUI equilibration procedure was used for all systems with the initial structure generated using CHARMM-GUI.[49,50] Replicas and other simulations initiated from already equilibrated configurations were started using randomly generated velocities without any further equilibration. Energy for Amber simulations with initial structures from CHARMM simulations were minimized before starting the simulation whenever required.

For CHARMM36 simulations, timestep of 2 fs was used, the temperature was coupled using a NosÃľâĂŞHoover thermostat,[56,57] the pressure was set to 1 bar with isotropic Par-

rinelloâĂŞRahman barostat,[58] particle mesh Ewald (PME) was used for electrostatic interactions at distances longer than 1.2 nm,[59,60] and Lennard-Jones interactions were cut off at 1.2 nm.

For simulations with Amber parameter, the timestep of 2 fs was used, the temperature was coupled using v-rescale thermostat, the pressure was set to 1 bar using isotropic Parrinello-RahmanâĂŞ barostat,[58] PME was used to calculate electrostatic interactions at distances longer than 1.0 nm,[59,60] and Lennard-Jones interactions were cut off at 1.0 nm.

Calculation of spin relaxation times from MD simulations and interpretation of underlying timescales

To couple spin relaxation times and molecular dynamics, we used Redfield equations[61] which connect T_1, T_2 and hetNOE spin relaxation times to the Fourier transformation (Spectral density) of the second-order rotational correlation functions of N-H, C-H or C-D bonds.[16,25] We calculated the rotational correlation functions, $C(t)$, for peptide backbone N-H bonds and C-H bonds in SDS molecules using the equation implemented in the gromacs package (gmx rotacf)[62]

$$C(t) = \left\langle \frac{3}{2}\cos^2\theta_{t'+t} - \frac{1}{2} \right\rangle_{t'}, \tag{1}$$

where $\theta_{t'+t}$ is the angle between bond vector at the times t and t'. To calculate the spectral density, we fitted a sum of exponential functions with the large number, N, of pre-fixed timescales, τ_i, to the correlation functions from simulations using the Python scipy optimize.nnls solver:

$$C_{\text{fit}}(t) = \sum_{i=1}^{N} \alpha_i e^{-t/\tau_i}. \tag{2}$$

For peptide N-H bonds, N=100 and τ_i values were equidistantly spaced in logarithmic scale between 1 ps and 100 ns. For SDS C-H bonds with a substantial amount of dynamics below

1 ps timescales, N=500 and τ_i values were equidistantly spaced in logarithmic scale between 1 fs and 1 μs. As a result, the fitting gives the weight, α_i, for each timescale that represents the relevance of the given timescale for the rotational relaxation of the bond. Spectral density, $J(\omega)$, is then obtained from the analytical Fourier transformation

$$J(\omega) = 2\int_0^\infty C_{\text{fit}}(t)cos(\omega t)\mathrm{d}t = 2\sum_{i=1}^{N}\alpha_i\frac{\tau_i}{1+\omega^2\tau_i^2} \tag{3}$$

and substituted into Redfield equations.[16,61] The spin relaxation time calculation is implemented in the python code available at `https://github.com/nencini/NMR_FF_tools/tree/master/relaxation_times`.

Correlation functions up to lag times (t in Eq. 1) of one-hundredth of the total simulation length were used when analysing the N-H peptide bonds, which should provide good statistics when analysing single molecule simulations.[63] For C-H bonds in SDS molecules, averaging over a larger number of molecules enables usage of lag times up to one-twentieth of the total simulation length. Small but non-zero weights (below ~1% in all systems except micelle simulations with Amber in gel-like phase with the weights below ~10%) for the slowest possible timescale (100 ns for peptide N-H bonds, 1 μs for SDS C-H bonds) were observed for some correlation functions. These artificial timescales, arising from incomplete equilibration of correlation functions to plateau to zero, were not taken into account in the analyses, although ignoring them did not have major effects on the spin relaxation times.

To comprise dynamic landscapes of peptides and detergent molecules in micelles, we describe the relevance of different timescales for rotational relaxation processes in different parts of molecules using the weights (α_i) for timescales (τ_i) resulting from the fit of Eq. 2 to the correlation functions calculated from simulations using Eq. 1. A similar analysis in our previous studies[15,16] gave dominant weights for the timescales reconciling with the overall rotation timescales for folded proteins, while most of the timescales had zero weights. For disordered protein regions, we observed more dispersed timescales without any dominant

motion.[15] These results indicate that the approach can detect relevant dynamic processes without any further assumptions. Here we interpret dynamic landscapes of peptides and detergents in micelles using the weights of each timescale that result from the fitting to correlation functions from simulations that give the best agreement with experiments. To better emphasize the essential timescale ranges, we merged weights of five consecutive timescales for the plots of dynamic landscapes.

Analysis of other properties

Effective correlation times used to characterize the average dynamical timescales of SDS molecules in micelles were calculated as an integral over rotational correlation functions

$$\tau_{\text{eff}} = \int_0^\infty C(t)\mathrm{d}t \approx \sum_{i=1}^{N} \alpha_i \tau_i. \tag{4}$$

To analyze the orientation of two peptides in the same micelle with respect to each other, we calculated the angle between the principal axes of the two peptides using the MDAnalysis package.[64,65] Rotational dynamics predicted by MD simulations were compared with the prediction for a spherical rigid body in a water media from the Stokes-Einstein equation

$$D_r = \frac{1}{6\pi\tau} = \frac{k_{\text{B}}T}{8\pi\eta r^3}, \tag{5}$$

where k_{B} is a Boltzmann constant, T is the temperature, η is the viscosity of water, r is the radius, D_r is the rotational diffusion coefficient, and τ is the timescale of the rotational dynamics of a rigid spherical object.[66] The radii of micelles were approximated using the radius of gyration. Because not all SDS molecules remain within a micelle throughout the simulation in some systems, we first determined which molecules are part of the micelle in simulations separately for each time step. This was done by selecting SDS molecules with any atom closer to any peptide atom than a cut-off distance of 1.4-1.8 nm. The cut-off distance was set system specifically to give the most reasonable results as exemplified for

eYqjD(TA) simulation with 50 SDS molecules in figure S3 where cut-off value 1.8 nm was used. The radii of gyrations were then calculated using these molecules together with the peptide(s) first separately for each configuration and then averaged over time. The number of SDS molecules in a micelle as a function of time was also used to monitor the equilibration of simulations as exemplified in figure S3. The average number of SDS molecules within a micelle in each simulation is reported in Tables S2 and S3. These analyses were performed with Python scripts utilizing the MDAnalysis package.[64,65]

Propensities of secondary structures in peptides were calculated using DSSP plug-in in Gromacs.[37,62] The propensity of individual secondary structural motives was averaged over the time of trajectories. The local environment helicity propensity of a residue was correlated with the T_1, T_2 and hetNOE value of the residue for all peptides and simulations. Local environment helicity is defined as an average over a given residue and its left and right neighbour if these exist (the end residues have either only the left neighbour or only the right neighbour). The correlation was characterized by the Pearson correlation coefficient and the corresponding p-value using the Pearson function from the Python scipy.stats package.

acknowledgement

The facilities and expertise of the HiLIFE NMR unit at the University of Helsinki, a member of Instruct-ERIC Centre Finland, FINStruct, and Biocenter Finland are gratefully acknowledged. We acknowledge CSC – IT Center for Science for computational resources. RN, MLGR, SMB, EM and OHSO thank the Academy of Finland for funding ((grant nos. 315596, 319902 & 345631)). CDD acknowledges funding by the European Research Council (StG637649), the Academy of Finland (331556), the Jane and Aatos Erkko Foundation (200057) and the Sigrid JusÃĺlius Foundation.

References

(1) Lozada, C.; Barlow, T. M. A.; Gonzalez, S.; Lubin-Germain, N.; Ballet, S. Identification and Characteristics of Fusion Peptides Derived From Enveloped Viruses. *Frontiers in Chemistry* **2021**, *9*.

(2) Bechinger, B.; Juhl, D. W.; Glattard, E.; Aisenbrey, C. Revealing the Mechanisms of Synergistic Action of Two Magainin Antimicrobial Peptides. *Frontiers in Medical Technology* **2020**, *2*.

(3) Huan, Y.; Kong, Q.; Mou, H.; Yi, H. Antimicrobial Peptides: Classification, Design, Application and Research Progress in Multiple Fields. *Frontiers in Microbiology* **2020**, *11*.

(4) Owji, H.; Nezafat, N.; Negahdaripour, M.; Hajiebrahimi, A.; Ghasemi, Y. A comprehensive review of signal peptides: Structure, roles, and applications. *European Journal of Cell Biology* **2018**, *97*, 422–441.

(5) Kuai, R.; Li, D.; Chen, Y. E.; Moon, J. J.; Schwendeman, A. High-Density Lipoproteins: NatureâĂŹs Multifunctional Nanoparticles. *ACS Nano* **2016**, *10*, 3015–3041.

(6) Denisov, I. G.; Sligar, S. G. Nanodiscs for structural and functional studies of membrane proteins. *Nat. Struct. Mol. Biol.* **2016**, *23*, 481–486.

(7) Strandberg, E.; Ulrich, A. S. NMR methods for studying membrane-active antimicrobial peptides. *Concepts in Magnetic Resonance Part A* **2004**, *23A*, 89–120.

(8) Hong, M. Structure, Topology, and Dynamics of Membrane Peptides and Proteins from Solid-State NMR Spectroscopy. *The Journal of Physical Chemistry B* **2007**, *111*, 10340–10351.

(9) Strandberg, E.; Ulrich, A. S. In *Modern Magnetic Resonance*; Webb, G. A., Ed.; Springer International Publishing: Cham, 2018; pp 1985–1996.

(10) Mandala, V. S.; Williams, J. K.; Hong, M. Structure and Dynamics of Membrane Proteins from Solid-State NMR. *Annual Review of Biophysics* **2018**, *47*, 201–222.

(11) GÃijnsel, U.; Hagn, F. Lipid Nanodiscs for High-Resolution NMR Studies of Membrane Proteins. *Chemical Reviews* **2022**, *122*, 9395–9421.

(12) Kay, L. E.; Torchia, D. A.; Bax, A. Backbone dynamics of proteins as studied by nitrogen-15 inverse detected heteronuclear NMR spectroscopy: application to staphylococcal nuclease. *Biochemistry* **1989**, *28*, 8972–8979.

(13) Jarymowycz, V. A.; Stone, M. J. Fast time scale dynamics of protein backbones: NMR relaxation methods, applications, and functional consequences. *Chemical reviews* **2006**, *106*, 1624–1671.

(14) Camacho-Zarco, A. R.; Schnapka, V.; Guseva, S.; Abyzov, A.; Adamski, W.; Milles, S.; Jensen, M. R.; Zidek, L.; Salvi, N.; Blackledge, M. NMR Provides Unique Insight into the Functional Dynamics and Interactions of Intrinsically Disordered Proteins. *Chemical Reviews* **2022**, *122*, 9331–9356.

(15) Virtanen, S. I.; Kiirikki, A. M.; Mikula, K. M.; Iwaï, H.; Ollila, O. S. Heterogeneous dynamics in partially disordered proteins. *Physical Chemistry Chemical Physics* **2020**, *22*, 21185–21196.

(16) Ollila, O. S.; Heikkinen, H. A.; Iwaï, H. Rotational dynamics of proteins from spin relaxation times and molecular dynamics simulations. *The Journal of Physical Chemistry B* **2018**, *122*, 6559–6569.

(17) McKay, M. J.; Martfeld, A. N.; De Angelis, A. A.; Opella, S. J.; Greathouse, D. V.; Koeppe, R. E. Control of Transmembrane Helix Dynamics by Interfacial Tryptophan Residues. *Biophysical Journal* **2018**, *114*, 2617–2629.

(18) Otera, H.; Wang, C.; Cleland, M. M.; Setoguchi, K.; Yokota, S.; Youle, R. J.; Mihara, K. Mff is an essential factor for mitochondrial recruitment of Drp1 during mitochondrial fission in mammalian cells. *Journal of Cell Biology* **2010**, *191*, 1141–1158.

(19) Keskin, A.; AkdoÄ§an, E.; Dunn, C. D. Evidence for Amino Acid Snorkeling from a High-Resolution, In Vivo Analysis of Fis1 Tail-Anchor Insertion at the Mitochondrial Outer Membrane. *Genetics* **2017**, *205*, 691–705.

(20) Lutfullahoğlu-Bal, G.; Keskin, A.; Seferoğlu, A. B.; Dunn, C. D. Bacterial tail anchors can target to the mitochondrial outer membrane. *Biology Direct* **2017**, *12*, 16.

(21) Kumar, V.; Butcher, S. J.; ÃŰÃűrni, K.; Engelhardt, P.; Heikkonen, J.; Kaski, K.; Ala-Korpela, M.; Kovanen, P. T. Three-Dimensional cryoEM Reconstruction of Native LDL Particles to 16ÃĚ Resolution at Physiological Body Temperature. *PLOS ONE* **2011**, *6*, 1–11.

(22) Shimobayashi, S. F.; Ohsaki, Y. Universal phase behaviors of intracellular lipid droplets. *Proceedings of the National Academy of Sciences* **2019**, *116*, 25440–25445.

(23) Hirose, T.; Ninomiya, K.; Nakagawa, S.; Yamazaki, T. A guide to membraneless organelles and their various roles in gene regulation. *Nature Reviews Molecular Cell Biology* **2023**, *24*, 288–304.

(24) Salomon-Ferrer, R.; Case, D. A.; Walker, R. C. An overview of the Amber biomolecular simulation package. *WIREs Computational Molecular Science* **2013**, *3*, 198–210.

(25) SÃűderman, O.; CarlstrÃűm, G.; Olsson, U.; Wong, T. C. Nuclear magnetic resonance relaxation in micelles. Deuterium relaxation at three field strengths of three positions on the alkyl chain of sodium dodecyl sulphate. *J. Chem. Soc., Faraday Trans. 1* **1988**, *84*, 4475–4486.

(26) Klauda, J. B.; Venable, R. M.; Freites, J. A.; OâĂŹConnor, J. W.; Tobias, D. J.; Mondragon-Ramirez, C.; Vorobyov, I.; MacKerell, A. D. J.; Pastor, R. W. Update of the CHARMM All-Atom Additive Force Field for Lipids: Validation on Six Lipid Types. *The Journal of Physical Chemistry B* **2010**, *114*, 7830–7843.

(27) Jorgensen, W. L.; Chandrasekhar, J.; Madura, J. D.; Impey, R. W.; Klein, M. L. Comparison of simple potential functions for simulating liquid water. *The Journal of Chemical Physics* **1983**, *79*, 926–935.

(28) Izadi, S.; Anandakrishnan, R.; Onufriev, A. V. Building Water Models: A Different Approach. *The Journal of Physical Chemistry Letters* **2014**, *5*, 3863–3871.

(29) Kadaoluwa Pathirannahalage, S. P.; Meftahi, N.; Elbourne, A.; Weiss, A. C. G.; McConville, C. F.; Padua, A.; Winkler, D. A.; Costa Gomes, M.; Greaves, T. L.; Le, T. C. et al. Systematic Comparison of the Structural and Dynamic Properties of Commonly Used Water Models for Molecular Dynamics Simulations. *Journal of Chemical Information and Modeling* **2021**, *61*, 4521–4536.

(30) Javanainen, M.; Lamberg, A.; Cwiklik, L.; Vattulainen, I.; Ollila, O. S. Atomistic model for nearly quantitative simulations of Langmuir monolayers. *Langmuir* **2018**, *34*, 2565–2572.

(31) Tempra, C.; Ollila, O. H. S.; Javanainen, M. Accurate Simulations of Lipid Monolayers Require a Water Model with Correct Surface Tension. *Journal of Chemical Theory and Computation* **2022**, *18*, 1862–1869.

(32) Rezaei-Ghaleh, N.; Parigi, G.; Soranno, A.; Holla, A.; Becker, S.; Schuler, B.; Luchinat, C.; Zweckstetter, M. Local and Global Dynamics in Intrinsically Disordered Synuclein. *Angewandte Chemie International Edition* **2018**, *57*, 15262–15266.

(33) Salvi, N.; Abyzov, A.; Blackledge, M. Multi-Timescale Dynamics in Intrinsically Dis-

ordered Proteins from NMR Relaxation and Molecular Simulation. *The Journal of Physical Chemistry Letters* **2016**, *7*, 2483–2489.

(34) Khan, S. N.; Charlier, C.; Augustyniak, R.; Salvi, N.; DÃĭjean, V.; Bodenhausen, G.; Lequin, O.; Pelupessy, P.; Ferrage, F. Distribution of Pico- and Nanosecond Motions in Disordered Proteins from Nuclear Spin Relaxation. *Biophysical Journal* **2015**, *109*, 988–999.

(35) Smith, A. A.; Ernst, M.; Meier, B. H. Optimized âĂIJdetectorsâĂİ for dynamics analysis in solid-state NMR. *The Journal of Chemical Physics* **2018**, *148*.

(36) Antila, H. S.; M. Ferreira, T.; Ollila, O. H. S.; Miettinen, M. S. Using Open Data to Rapidly Benchmark Biomolecular Simulations: Phospholipid Conformational Dynamics. *Journal of Chemical Information and Modeling* **2021**, *61*, 938–949.

(37) Kabsch, W.; Sander, C. Dictionary of protein secondary structure: Pattern recognition of hydrogen-bonded and geometrical features. *Biopolymers* **1983**, *22*, 2577–2637.

(38) StenstrÃűm, O.; Champion, C.; Lehner, M.; Bouvignies, G.; Riniker, S.; Ferrage, F. How does it really move? Recent progress in the investigation of protein nanosecond dynamics by NMR and simulation. *Current Opinion in Structural Biology* **2022**, *77*, 102459.

(39) Kemper, C.; Habib, S. J.; Engl, G.; Heckmeyer, P.; Dimmer, K. S.; Rapaport, D. Integration of tail-anchored proteins into the mitochondrial outer membrane does not require any known import components. *Journal of Cell Science* **2008**, *121*, 1990–1998.

(40) Krumpe, K.; Frumkin, I.; Herzig, Y.; Rimon, N.; Özbalci, C.; Brügger, B.; Rapaport, D.; Schuldiner, M. Ergosterol content specifies targeting of tail-anchored proteins to mitochondrial outer membranes. *Molecular Biology of the Cell* **2012**, *23*, 3927–3935.

(41) Ozgur, B.; Dunn, C. D.; Sayar, M. Modeling Adsorption, Conformation, and Orientation of the Fis1 Tail Anchor at the Mitochondrial Outer Membrane. *Membranes* **2022**, *12*.

(42) Antila, H. S.; Kav, B.; Miettinen, M. S.; Martinez-Seara, H.; Jungwirth, P.; Ollila, O. H. S. Emerging Era of Biomolecular Membrane Simulations: Automated Physically-Justified Force Field Development and Quality-Evaluated Databanks. *The Journal of Physical Chemistry B* **2022**, *126*, 4169–4183.

(43) Kiirikki, A.; Antila, H.; Bort, L.; Buslaev, P.; Fernando, F.; Mendes Ferreira, T.; Fuchs, P.; Garcia-Fandino, R.; Gushchin, I.; Kav, B. et al. NMRlipids Databank makes data-driven analysis of biomembrane properties accessible for all. *ChemRxiv* **2023**,

(44) Tiemann, J. K. S.; Szczuka, M.; Bouarroudj, L.; Oussaren, M.; Garcia, S.; Howard, R. J.; Delemotte, L.; Lindahl, E.; Baaden, M.; Lindorff-Larsen, K. et al. MDverse: Shedding Light on the Dark Matter of Molecular Dynamics Simulations. *bioRxiv* **2023**,

(45) Skinner, S. P.; Fogh, R. H.; Boucher, W.; Ragan, T. J.; Mureddu, L. G.; Vuister, G. W. CcpNmr AnalysisAssign: a flexible platform for integrated NMR analysis. *Journal of Biomolecular NMR* **2016**, *66*, 111–124.

(46) Hinds, M. G.; Norton, R. S. NMR spectroscopy of peptides and proteins: Practical considerations. *Molecular biotechnology* **1997**, *7*, 315–331.

(47) Barbato, G.; Ikura, M.; Kay, L. E.; Pastor, R. W.; Bax, A. Backbone dynamics of calmodulin studied by nitrogen-15 relaxation using inverse detected two-dimensional NMR spectroscopy: the central helix is flexible. *Biochemistry* **1992**, *31*, 5269–5278.

(48) Farrow, N. A.; Muhandiram, R.; Singer, A. U.; Pascal, S. M.; Kay, C. M.; Gish, G.; Shoelson, S. E.; Pawson, T.; Forman-Kay, J. D.; Kay, L. E. Backbone Dynamics of a

Free and a Phosphopeptide-Complexed Src Homology 2 Domain Studied by 15N NMR Relaxation. *Biochemistry* **1994**, *33*, 5984–6003.

(49) Cheng, X.; Jo, S.; Lee, H. S.; Klauda, J. B.; Im, W. CHARMM-GUI Micelle Builder for Pure/Mixed Micelle and Protein/Micelle Complex Systems. *Journal of Chemical Information and Modeling* **2013**, *53*, 2171–2180.

(50) Lee, J.; Cheng, X.; Swails, J. M.; Yeom, M. S.; Eastman, P. K.; Lemkul, J. A.; Wei, S.; Buckner, J.; Jeong, J. C.; Qi, Y. et al. CHARMM-GUI Input Generator for NAMD, GROMACS, AMBER, OpenMM, and CHARMM/OpenMM Simulations Using the CHARMM36 Additive Force Field. *Journal of Chemical Theory and Computation* **2016**, *12*, 405–413.

(51) DubouÃľ-Dijon, E.; Javanainen, M.; Delcroix, P.; Jungwirth, P.; Martinez-Seara, H. A practical guide to biologically relevant molecular simulations with charge scaling for electronic polarization. *The Journal of Chemical Physics* **2020**, *153*, 050901.

(52) PluhaÅŹovÃą, E.; Fischer, H. E.; Mason, P. E.; Jungwirth, P. Hydration of the chloride ion in concentrated aqueous solutions using neutron scattering and molecular dynamics. *Molecular Physics* **2014**, *112*, 1230–1240.

(53) Abraham, M. J.; Murtola, T.; Schulz, R.; Páll, S.; Smith, J. C.; Hess, B.; Lindahl, E. GROMACS: High performance molecular simulations through multi-level parallelism from laptops to supercomputers. *SoftwareX* **2015**, *1*, 19–25.

(54) Páll, S.; Abraham, M. J.; Kutzner, C.; Hess, B.; Lindahl, E. Tackling exascale software challenges in molecular dynamics simulations with GROMACS. Solving Software Challenges for Exascale: International Conference on Exascale Applications and Software, EASC 2014, Stockholm, Sweden, April 2-3, 2014, Revised Selected Papers 2. 2015; pp 3–27.

(55) Sousa da Silva, A. W.; Vranken, W. F. ACPYPE - AnteChamber PYthon Parser interfacE. *BMC Research Notes* **2012**, *5*, 367.

(56) Nosé, S. A unified formulation of the constant temperature molecular dynamics methods. *The Journal of chemical physics* **1984**, *81*, 511–519.

(57) Hoover, W. G. Canonical dynamics: Equilibrium phase-space distributions. *Physical review A* **1985**, *31*, 1695.

(58) Parrinello, M.; Rahman, A. Polymorphic transitions in single crystals: A new molecular dynamics method. *Journal of Applied physics* **1981**, *52*, 7182–7190.

(59) Darden, T.; York, D.; Pedersen, L. Particle mesh Ewald: An N. log (N) method for Ewald sums in large systems. *The Journal of chemical physics* **1993**, *98*, 10089–10092.

(60) Essmann, U.; Perera, L.; Berkowitz, M. L.; Darden, T.; Lee, H.; Pedersen, L. G. A smooth particle mesh Ewald method. *The Journal of chemical physics* **1995**, *103*, 8577–8593.

(61) Abragam, A. *The Principles of Nuclear Magnetism*; Oxford University Press, 1961.

(62) Abraham, M.; Alekseenko, A.; Bergh, C.; Blau, C.; Briand, E.; Doijade, M.; Fleischmann, S.; Gapsys, V.; Garg, G.; Gorelov, S. et al. GROMACS 2023.1 Manual. 2023; `https://doi.org/10.5281/zenodo.7852189`.

(63) Lu, C.-Y.; Vanden Bout, D. A. Effect of finite trajectory length on the correlation function analysis of single molecule data. *The Journal of chemical physics* **2006**, *125*, 124701.

(64) Gowers, R. J.; Linke, M.; Barnoud, J.; Reddy, T. J.; Melo, M. N.; Seyler, S. L.; Domanski, J.; Dotson, D. L.; Buchoux, S.; Kenney, I. M. et al. MDAnalysis: a Python package for the rapid analysis of molecular dynamics simulations. Proceedings of the 15th python in science conference. 2016; p 105.

(65) Michaud-Agrawal, N.; Denning, E. J.; Woolf, T. B.; Beckstein, O. MDAnalysis: a toolkit for the analysis of molecular dynamics simulations. *Journal of computational chemistry* **2011**, *32*, 2319–2327.

(66) Woessner, D. E. Nuclear Spin Relaxation in Ellipsoids Undergoing Rotational Brownian Motion. *J. Chem. Phys.* **1962**, *37*, 647–654.